Role of impact ionization and self-consistent tunnel injection in Schottky-barrier diodes operating under strong reverse-bias conditions

Tomás González*, Beatriz Orfao, Susana Pérez, Javier Mateos, and Beatriz G. Vasallo

Departamento de Física Aplicada and USAL-NANOLAB, Universidad de Salamanca, 37008 Salamanca, Spain

E-mail: tomasg@usal.es

This work shows that for a correct analysis of Schottky barrier diodes operating under strong reverse-bias conditions it is necessary to account for the self-consistency between the shape of the energy barrier and carrier concentration in the depletion region, since the full-depletion approximation fails to estimate the current. This happens for very high applied voltages, at which impact ionization by electrons and holes must also be considered. Two example GaN diodes with different doping concentration and barrier height are analyzed. The results are relevant to regions of the diodes where a very high tunnel injection takes place, like the contact edge or surface inhomogeneities.

Schottky-barrier diodes (SBDs) based on wide-bandgap semiconductors, like SiC, GaN and Ga_2O_3, have attracted increasing attention in last years because of to their capability to handle high power.[1,2] Among them, GaN, thanks to its high electron mobility, is an excellent candidate for high-frequency, high-power, and high-temperature applications.[3] A key parameter for the performance of SBDs in these applications is the breakdown voltage.[4,5,6] In vertical devices, values of the breakdown voltage lower than that theoretically expected are typically found.[7] A variety of mechanisms, mostly associated to traps and defects in the epilayer, like trap assisted tunneling, Poole Frenkel emission, variable range hoping, etc., lead to enhanced values of the reverse leakage current with respect to that originated by the ideal thermionic emission (TE) and tunneling current (TC) contributions.[8,9] The use of native substrates in GaN-on-GaN SBDs allows reducing a lot these defects,[10,11] but still a premature breakdown may take place due to the crowding of the electric field at the Schottky contact (SC) edge.[12] Extremely high values of the electric field can be found at the interface between the metal and the semiconductor,[13] which boost up the tunneling current and originate impact ionization (II) processes initiated by the tunneled electrons.[14] Local high values of the tunneling current can also be found due to inhomogeneities in the barrier height, frequently found in experiments and attributed to a poor surface quality of the GaN epilayer or to the microstructure of the metal/GaN interface.[15]

The models typically used to analyze the ideal leakage-current contributions, associated to TE and TC, assume full depletion (FD) in the semiconductor region adjacent to the metal to determine the profile of the energy barrier through which electrons tunnel.[16,17] Some basic models assume a triangular barrier determined by the electric field at the interface,[18] while more sophisticated ones include the correction associated to the doping of the epilayer, important in the case of highly-doped SBDs.[19] The assumption of FD used by all these models is valid as long as the tunnel current reaches relatively low values, so that the carrier concentration in the depletion region associated to the injected electrons is negligible with respect to the doping concentration. They are used, for example, to estimate the rated blocking voltage of SBDs,[19] or the transition between different transport regimes.[20,21]

However, in regions of the diode surface where a very high electric field is present (contact edges) or the barrier height is much lower than the nominal one (inhomogeneities), the amount of injected electrons may be locally so high that the FD assumption does not hold anymore. In such a case, the barrier profile determining electron tunnel injection must be self-consistently calculated with carrier concentration in the depletion region, thus being necessary the simulation of carrier transport. In particular, under so high electric fields like those reached at the contact edges, II initiated by the injected electrons, and also by the generated holes, must be carefully considered, as it may lead to significant increase of carrier concentration and ultimately provoke avalanche breakdown of the SBDs.[22,23,24] This subject is of high importance, since the breakdown voltage or maximum surface electric field (E_{max}) of SBDs may become limited by the leakage current rather than the material's breakdown electric field.

The aim of this work is to show that under high enough reverse bias voltages, in order to correctly calculate the tunneling current through the contact it is necessary to go beyond the FD approximation and account for the self-consistency between the shape of the energy barrier and the carrier concentration in the depletion region. To this end, apart from the tunnel current at the SC, a transport model for electrons and holes must be considered, which, in case of dealing with very high electric fields, should include II. In our case, a homemade Monte Carlo (MC) simulator coupled to a one-dimensional Poisson's solver will be used, which has already been successfully exploited for the simulation of SBDs.[25,26] Despite in some specifically designed devices, like avalanche photodiodes based on periodically stacked GaN/AlN structures,[27,28] II is unipolar (only provoked by electrons), in a general case hole-initiated II is also significant in GaN devices. [22,23,24,29] Theoretical studies indicate that hole-initiated II becomes dominant for field strengths about 3.0 MV/cm[30,31], attained in the devices we will analyze. Thus, in our model we will consider II not only initiated by electrons, but also by holes.

As prototypes to analyze this problem we will consider two GaN diodes consisting in a homogeneous n-type semiconductor with ohmic and SCs at their left- and right-side ends, respectively. Diode A has a length of 2.5 μm, a doping of 10^{17} cm^{-3} and a barrier height of 0.935 eV. It will be analyzed at 450 K, temperature at which *I-V* curves replicating the ideal behavior associated to TE and TC contributions have been measured.[32] In the case of diode B, the length is 1.0 μm, the doping 4×10^{17} cm^{-3} and the barrier height 0.6 eV, and it will be analyzed at 300 K. The MC model for electrons in the conduction band and the corresponding parameters are the same as in Ref. 33. II is modeled using the Keldysh approach,[34,35] with a probability per unit time given by: $P(\varepsilon) = S[(\varepsilon - \varepsilon_{th})/\varepsilon_{th}]^2$ when $\varepsilon > \varepsilon_{th}$ and 0 otherwise, where ε is the carrier kinetic energy, ε_{th} the ionization threshold energy (here 3.0 eV for both electrons and holes), and S is a measure of the softness or hardness of the threshold (here 5×10^{12} s^{-1} for electrons and 2.5×10^{13} s^{-1} for holes). As a result of II, holes will be present in the diodes and may play a key role. The MC model for holes in the valence band, scattering mechanisms and corresponding parameters are the same as in Ref. 34, except the effective masses of heavy and light holes, which in our case are 1.3 and 1.1, respectively. As concerns tunnel injection at the SC, we use the model developed in Ref. 32 (including a detailed treatment of image charge barrier lowering), except that for the calculation of the tunnel injection rate at each energy, instead of the potential barrier profile given by the FD approximation, in MC simulations we consider the profile resulting from the self-consistent solution of Poisson's equation.[36,37] In order to correctly solve Poisson's equation and accurately account for tunnel injection, we use a time step of 2.5 fs and cells of sub-nm length near the SC. With the aim of identifying the influence of self-consistency and II, MC simulations in which tunnel injection and/or II are switched off will also be performed. MC results will be compared with the ideal values of the reverse current (TE and TC components) obtained numerically with the barrier profile given by the FD assumption.[32)]

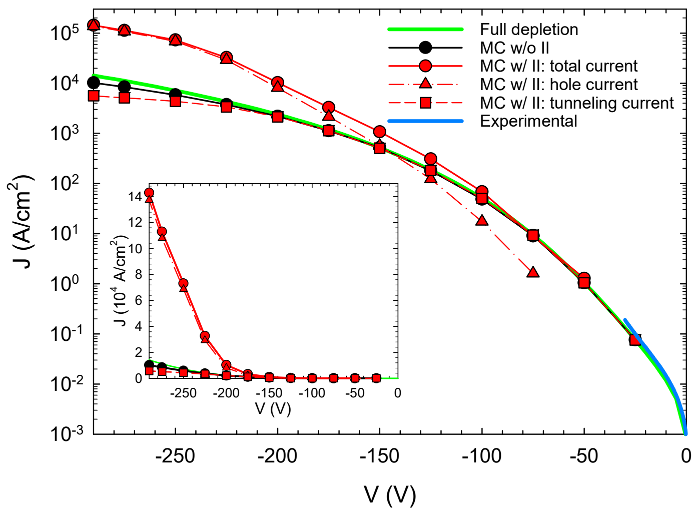

Fig. 1. *I-V* curve under reverse bias conditions for diode A at 450 K calculated by three different models (FD assumption, MC without II and MC with II) jointly with hole and tunneling contributions at the SC in the case of MC with II. Experimental measurements from Ref. 32 are also shown. The inset shows the same results in linear scale to better evidence the current increase.

The simulated *I-V* curves of diode A at 450 K are shown in Fig. 1. When the reverse bias is lower than 100 V, the electron concentration in the depletion region is still small as compared to the doping concentration and II is negligible, so that, as observed, all the models essentially coincide with the FD results. Experimental values in this bias range (also shown in the figure) were measured in a previous work, finding a good agreement with the FD predictions.[32)] For voltages between -100 and -175 V, even if the tunnel injection at the SC (squares) still matches the FD values, the overall current (red circles) is higher than the FD estimation due to the increasing contribution to the current of the carriers generated by II events (triangles), calculated as the hole current at the SC, which, for voltages beyond -175 V, becomes dominant. At the highest voltages, even if electron tunnel injection from the SC is lower than that expected from them FD approximation, the intense generation of electrons and holes by II leads to a sharp increase of the current (see the inset in linear scale), which would ultimately lead to the (avalanche) breakdown of the diode.

Figs. 2 to 4 illustrate the interpretation given above. Fig. 2 shows how, for high enough applied voltages, electrons tunneled at the SC gain energy from the very high field inside the device and generate II events as they drift left. As the applied voltage is raised, the II events are more frequent and extend over a longer region. Generated holes, in turn, gain enough energy while moving right towards the SC to also originate II processes. Remarkably, for the highest voltages (-250 V in Fig. 2), the hole II rate exceeds that of electrons in the vicinity of the SC. At -175 V, as observed in the profiles of carrier concentration shown in Fig. 3(a) by dashed lines, the hole concentration originated by II is comparable to the electron concentration near the SC and contributes to increase the current, but both concentrations are still low as to modify the shape of the energy barrier. In contrast, for -275 V, solid lines in Fig. 3(a), hole and electron concentrations in the theoretical depletion region become so high that they are of the order of the doping concentration and the shape of the electric field and the potential energy barrier changes [see Fig. 3(b) and its inset]. The barrier becomes wider with respect to the FD shape, as corresponds to the lower value of $E_{\max}$ at the contact, and so tunnel injection is smaller than the FD prediction (Fig. 1). If the reverse bias is further increased, more frequent II events lead to a continuing raise of carrier density inside the device that would ultimately lead to avalanche breakdown. Note that an essential element for correctly describing this situation is the self-consistent consideration of tunnel injection and carrier concentration in the depletion region.

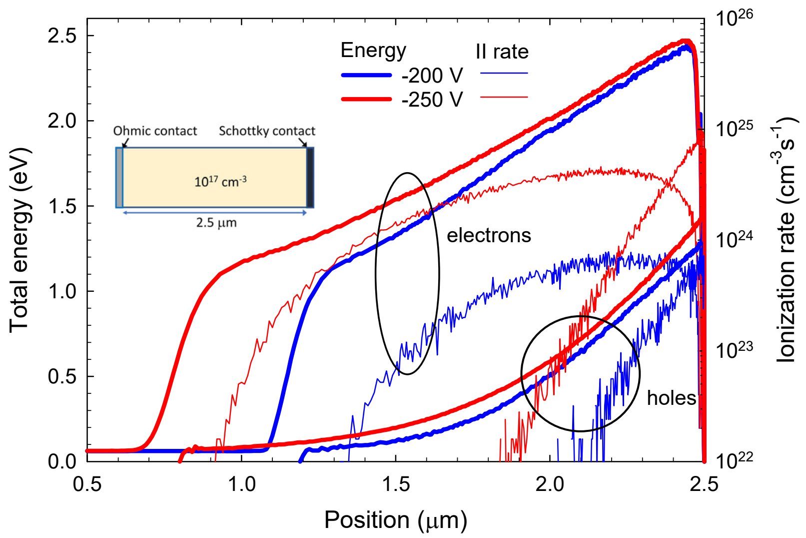

Fig. 2. Profiles of total average energy and II rate of electrons and holes in diode A for bias voltages of -200 and -250 V. The inset shows the positions of the ohmic (x=0 μm) and Schottky (x=2.5 μm) contacts in the diode.

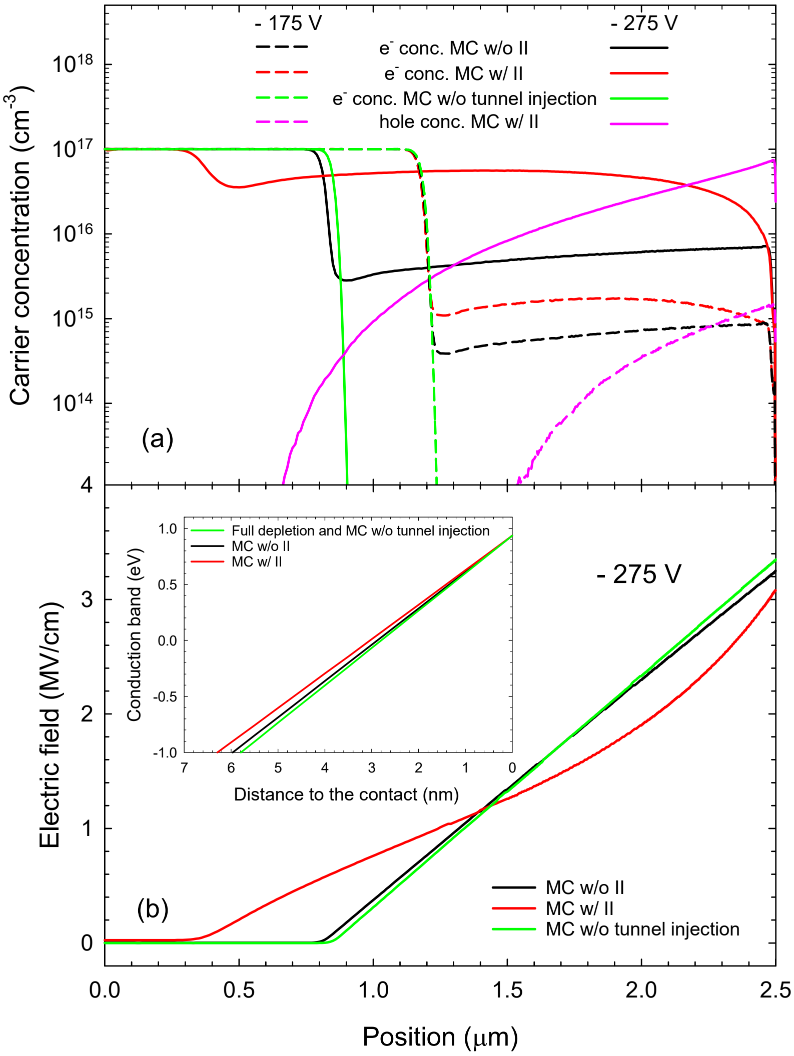

Fig. 3. (a) Profiles of electron concentration in diode A at 450 K for applied voltages of -175 V (dashed lines) and -275 V (solid lines) calculated with and without considering II in MC simulations. The MC results without tunnel injection from the SC are also shown for comparison. Hole concentration in the case of considering II is also plotted. (b) Corresponding electric field profiles for the case of -275 V. The inset in (b) shows the conduction band at the SC for the same cases (taking the metal Fermi level as zero-energy reference) compared with the FD approximation, which exactly coincides with the MC results without tunnel injection.

The values of E_{max} as a function of the applied voltage are shown in Fig. 4. As observed, E_{max} departs from the FD estimation for voltages beyond -200 V, reaching values below the critical electric field of GaN (3.4 MV/cm)[29] within the voltage range under analysis. In the case when II is not considered in the simulations, at the highest voltages, the current level (black circles in Fig. 1) is slightly lower than that predicted with the FD approximation, since the increasing carrier concentration in the depletion region associated to a more pronounced tunnel injection [see black lines in Fig. 3(a)] leads to a bit wider energy barrier at the contact (lower E_{max}). When II is considered, despite the total current (red circles in Fig. 1) is much higher than that predicted by the FD approximation due to the contribution of carriers generated by II (red triangles in Fig. 1), the tunneling current is even smaller that in the absence of II because of the lower E_{max}. This is due to the influence of the increasing negative charge associated to the electrons generated by II [red lines in Fig. 3(a)], which is not compensated by the (also increasing) presence of holes near the SC.

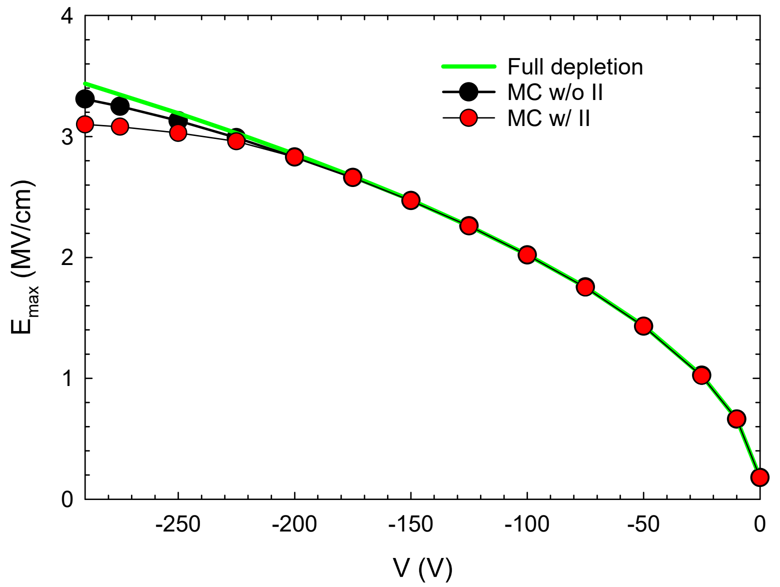

Fig. 4. Maximum electric field (at the semiconductor-metal interface) as a function of the reverse-bias voltage calculated in diode A with and without considering II compared with the FD estimation.

The electron concentration calculated without tunnel injection [green curves in Fig. 3(a)] shows a sharp decrease at the position corresponding to the edge of the depletion region, which coincides exactly with that obtained assuming FD. As observed in Fig. 3(a), at low voltages the width of the depletion region is not modified by tunnel injection nor the presence of II (dashed lines), however it increases with respect to the FD case at the highest voltages (solid lines), when the carrier concentration is so large that the potential drop is no longer quadratic [solid red line in Fig. 3(b)].

A different scenario is found in the results corresponding to diode B, where a higher doping of 4×10^{17} cm^{-3}, similar to that of diodes used in high-frequency multipliers,[38] and a lower energy barrier of 0.6 eV, which could be attributed to a local inhomogeneity, are considered. Under these conditions, strong tunnel injection (associated to a high E_{max}) takes place at lower values of reverse bias voltage than in diode A, so that II events are expected to be less intense. The *I-V* curves obtained in this diode under different simulation conditions are shown in Fig. 5. The first significant difference with respect to diode A is the strong reduction of the current level in absence of II (black circles) with respect to the FD estimation, taking place from relatively low voltages (beyond -30 V). As shown in the profiles of Fig. 6 (corresponding to -90 V), even in the absence of II, electron concentration in the depletion region is so high that the energy barrier widens with respect to the FD case (lower E_{max}) and tunneling current decreases. The onset of II and the associated increase of carrier concentration as the applied voltage is raised originate a change of the electric field profile, but, interestingly, the width of the barrier and the value of E_{max} remain the same [see Fig. 6(b) and its inset]. Remarkably, in contrast to the case of diode A, despite the increasing contribution to the current of carriers generated by II (triangles in Fig. 5), in no case the current level (red circles) exceeds that obtained with the FD assumption, and no tendency to breakdown is observed (even if a thermal process related to self-heating, not simulated here, could lead to the avalanche). This situation holds up to the highest applied voltages, with E_{max} reaching a saturation value lower than the critical electric field of GaN (inset of Fig. 5) and considerably smaller than the FD values as compared to the case of diode A.

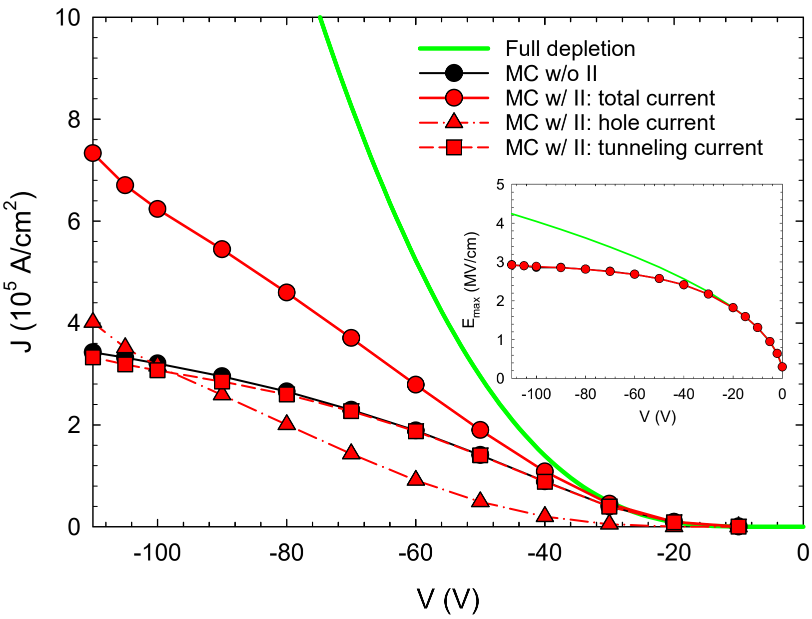

Fig. 5. *I-V* curve under reverse bias conditions for diode B calculated by three different models (FD assumption, MC without II and MC with II) jointly with hole and tunneling contributions at the SC in the case of MC with II. The inset shows the maximum electric field (at the semiconductor-metal interface) obtained with and without considering II (which coincide) compared with the FD estimation.

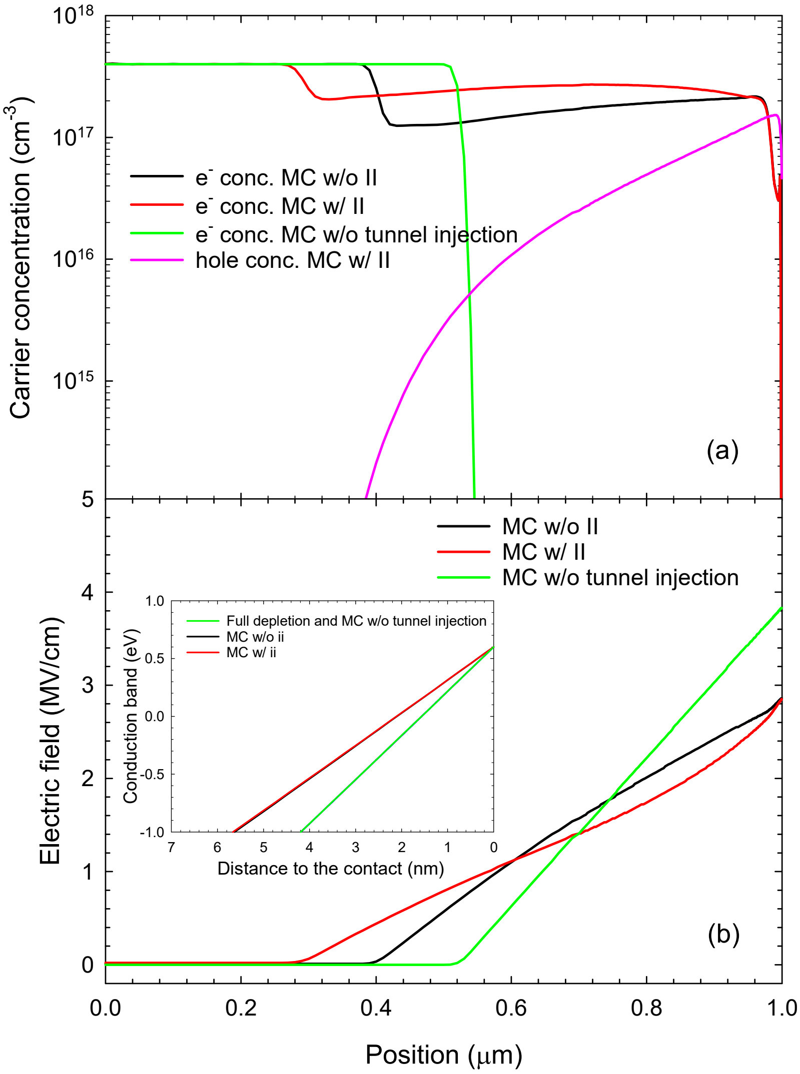

Fig. 6. (a) Profiles of electron concentration in diode B for an applied voltage of -90 V calculated with and without considering II in MC simulations. The MC results without tunnel injection from the SC are also shown for comparison. Hole concentration in the case of considering II is also plotted. (b) Corresponding electric field profiles. The inset in (b) shows the conduction band at the SC for the same cases (taking the metal Fermi level as zero-energy reference) compared with the FD approximation, which exactly coincides with the MC results without tunnel injection.

We must remark that, apart from the model and parameters adopted for II, a key factor determining the hole concentration near the SC is the high-field hole velocity, for which different values can be found in the literature.[30,34] Faster (slower) holes would lead to a reduced (enhanced) hole concentration, thus decreasing (increasing) their influence on the observed phenomena and modifying the voltage range were such phenomena take place.

The reverse *I-V* curves shown in this work do not include the influence of the series resistance, which is not critical. In the case of large-surface diodes, a size-independent series resistance can be assumed. Considering a typical value of 10 Ω, for current densities as high as 10^5 A/cm^2 as those reached in this work, for the voltage drop in the series resistance to be larger than 10 V, the diode diameter should be higher than about 35 μm. In the case of small-surface diodes, the series resistance is mainly associated to the epilayer and thus inversely proportional to their surface. According to the features of the diodes under analysis, for current densities of 10^5 A/cm^2, the voltage drop in the series resistance would be about 3 V in diode A and 0.15 V in diode B regardless of the diode surface.

In summary, by means of MC simulations of GaN SBDs including a detailed treatment of tunnel injection at the SC, we have shown that for a correct prediction of the *I-V* curves at high applied voltages in reverse bias, the shape of the barrier and the associated tunnel injection must be self-consistently calculated with carrier concentration in the depletion region accounting for II-generated electrons and holes. The voltage range at which these effects are relevant and the relative influence of tunnel injection and II depend on the doping of the epilayer and the barrier height. We remark that the effects described in this work are likely to be present just in some specific regions of SBDs, like the contact edge or surface inhomogeneities, where very high current densities and/or electric fields are locally reached, without necessarily leading to a global breakdown of the device.

Acknowledgments

This work has been partially supported through Grant PID2020-115842RB-I00 funded by MCIN/AEI/10.13039/501100011033. B. Orfao acknowledges the PhD contract from the Junta de Castilla y León.

References

1) F. Roccaforte, P. Fiorenza, G. Greco, R. Lo Nigro, F. Giannazzo, F. Iucolano, and M. Saggio, Microelectron. Eng. **187-188**, 66 (2018).

2) S. Pearton, F. Ren, and M. Mastro, Eds., *Gallium Oxide Technology, Devices and Applications* (Elsevier, Oxford, 2019).

3) H. Fu, K. Fu, S. Chowdhury, T. Palacios, and Y. Zhao, IEEE Trans. Electron. Dev. **68**, 3200 (2021).

4) X. Guo, Y. Zhong, X. Chen, Y. Zhou, S. Su, S. Yan, J. Liu, X. Sun, Q. Sun, and H. Yang, Appl. Phys. Lett. **118**, 243501 (2021).

5) F. Huang, X. Jia, Y. Liu, K. Tian, C. Chu, Q. Zheng, Y. Zhang, Z. Xin, Z.-H. Zhang, and Q. Li, AIP Advances **11**, 045316 (2021).

6) F. Huang, C. Chu, X. Jia, K. Tian, Y. Zhang, Q. Zheng, Q. Li, and Z.-H. Zhang, Jpn. J. Appl. Phys. **61**, 014002 (2022).

7) L. Sang, B. Ren, M. Sumiya, M. Liao, Y. Koide, A. Tanaka, Y. Cho, Y. Harada, T. Nabatame, T. Sekiguchi, S. Usami, Y. Honda, and H. Amano, Appl. Phys. Lett. **111**, 122102 (2017).

8) K. Fu, H. Fu, X. Huang, T. Yang, C. Cheng, P.R. Peri, H. Chen, J. Montes, C. Yang, J. Zhou, X. Deng, X. Qi, D. J. Smith, S. M. Goodnick and Y. Zhao, IEEE J. Electron Devices Soc. **8**, 74 (2020).

9) J. Chen, Z. Liu, H. Wang, X. Song, Z. Bian, X. Duan, S. Zhao, J. Ning, J. Zhang, and Y. Hao, Appl. Phys. Express **14**, 104002 (2021).

10) J. Suda, K. Yamaji, Y. Hayashi, T. Kimoto, K. Shimoyama, H. Namita, and S. Nagao, Appl. Phys. Express **3,** 101003 (2010).

11) Y. Saitoh, K. Sumiyoshi, M. Okada, T. Horii, T. Miyazaki, H. Shiomi, M. Ueno, K. Katayama, M. Kiyama, and T. Nakamura, Appl. Phys. Express **3**, 081001 (2010).

12) X. Liu, F. Lin, J. Li , Y. Lin, J. Wu, H. Wang, X. Li, S. Huang, Q. Wang, H.-C. Chiu, and H. C. Kuo, IEEE Trans. Electron. Dev. **69**, 1938 (2022).

13) B. Orfao , B. G. Vasallo, S. Pérez, J. Mateos, D. Moro-Melgar, M. Zaknoune, and T. González, IEEE Trans Electron Dev. **68**, 4296 (2021).

14) X. Liu, H. Gu, K. Li, J. Wang, L. Wang, H. C. Kuo, W. Liu, L. Chen, J. Fang, M. Liu, X. Lin, K. Xu, and J. P. Ao, ECS J. Solid State Sci. **6**, N216 (2017).

15) F. Roccaforte, F. Giannazzo, A. Alberti, M. Spera, M. Cannas, I. Cora, B. Pécz, F. Iucolano, and G. Greco, Mater. Sci. Semicond. **94**, 164 (2019).

16) F. A. Padovani and R. Stratton, Solid State Electron. **9**, 695 (1966).
17) A. Latreche, Semicond. Phys. Quantum Electron. Optoelectron. **22**, 397 (2017).
18) J. Nicholls, S. Dimitrijev, P. Tanner and J. Han, Sci. Rep. **9**, 3754 (2019).
19) W. Li, D. Saraswat, Y. Long, K. Nomoto, D. Jena, and H. G. Xing, Appl. Phys. Lett. **116**, 192101 (2020).
20) W. Li, K. Nomoto, D. Jena, and H. G. Xing, Appl. Phys. Lett. **117**, 222104 (2020).
21) M. Hara, H. Tanaka, M. Keneko, and T. Kimoto, Appl. Phys. Lett. **120**, 172103 (2022).
22) L. Cao, J. Wang, G. Harden, H. Ye, R. Stillwell, A. J. Hoffman, and P. Fay, Appl. Phys. Lett. **112**, 262103 (2018).
23) D. Ji, B. Ercan, and S. Chowdhury, Appl. Phys. Lett. **115**, 073503 (2019).
24) D. Ji and S. Chowdhury, Appl. Phys. Lett. **117**, 252107 (2020).
25) T. González, D. Pardo, L. Varani, and L. Reggiani, Appl. Phys. Lett. **63**, 3040 (1993).
26) D. Pardo, J. Grajal, S. Pérez, B. Mencía, J. Mateos, and T González, Semicond. Sci. Technol **26**, 055023 (2011).
27) J. Zheng, L. Wang, X. Wu, Z. Hao, C. Sun, B. Xong, Y. Luo, Y. Han, J. Wnag, H. Li, J. Brault, S. Matta, M. Al Khalfioui, J. Yan, T. Wei, Y. Zhang, and J. Wang, Appl. Phys. Lett. **109**, 241105 (2016).
28) J. Kang, Q. Li, and Y. Wan, J. Phys. D: Appl. Phys. **54**, 285107 (2021).
29) T. Maeda, T. Narita, S. Yamada, T. Kachi, T. Kimoto, M. Horita, and J. Suda, J. Appl. Phys. **129**, 185702 (2021).
30) F. Bertazzi, M. Moresco, and E. Bellotti, J. Appl. Phys. **106**, 063718 (2009).
31) M. Moresco, F. Bertazzi, and E. Bellotti, J. Appl. Phys. **106**, 063719 (2009).
32) B. Orfao, G. Di Gioia, B. G. Vasallo, S. Pérez, J. Mateos, Y. Roelens, E. Frayssinet, Y. Cordier, M. Zaknoune, and T. González, J. Appl. Phys. **132**, 044502 (2022).
33) S. García, S. Pérez, I. Íñiguez-de-la-Torre, J. Mateos, and T. González, J. Appl. Phys. **115**, 044510 (2014).
34) S. Chen and G. Wang, J. Appl. Phys. **103**, 023703 (2008).
35) B. G. Vasallo, T. González, V. Talbo, Y. Lechaux, N. Wichmann, S. Bollaert, and J. Mateos, J. Appl. Phys. **123**, 034501 (2018).
36) L. Sun, X. Y. Liu, M. Liu, G. Du, and R. Q. Han, Semicond. Sci. Technol. **18**, 576 (2003).
37) E. Pascual, R. Rengel, and M. J. Martín, Semicond. Sci. Technol. **22**, 1003 (2007).
38) L. Zhang, S. Liang , Y. Lv, D. Yang, X. Fu, X. Song, G. Gu, P. Xu, Y. Guo, A. Bu, Z. Feng, and S. Cai, IEEE Electron Device Lett. **42**, 1588 (2021).